

Journal of Materials Chemistry A

Accepted Manuscript



This is an *Accepted Manuscript*, which has been through the Royal Society of Chemistry peer review process and has been accepted for publication.

Accepted Manuscripts are published online shortly after acceptance, before technical editing, formatting and proof reading. Using this free service, authors can make their results available to the community, in citable form, before we publish the edited article. We will replace this *Accepted Manuscript* with the edited and formatted *Advance Article* as soon as it is available.

You can find more information about *Accepted Manuscripts* in the [Information for Authors](#).

Please note that technical editing may introduce minor changes to the text and/or graphics, which may alter content. The journal's standard [Terms & Conditions](#) and the [Ethical guidelines](#) still apply. In no event shall the Royal Society of Chemistry be held responsible for any errors or omissions in this *Accepted Manuscript* or any consequences arising from the use of any information it contains.

Rational Design of Hybrid Dye-Sensitized Solar Cells Composed of Double-layered Photoanodes with Enhanced Power Conversion Efficiency

Xiaodan Zhang^{a,b}, Wenming Liao^a, Wei Mu^{b,c}, Dajiang Zheng^a, Yusheng Zhou^a, Bailiang, Xue^b, Wei Liu^c, Zhiqun Lin^a, Yulin Deng^{b,c,*}

^a School of Materials Science and Engineering

^b Institute of Paper Science & Technology

^c School of Chemical & Biomolecular Engineering

Georgia Institute of Technology, Atlanta, GA 30318, United States

* Author for correspondence (E-mail: yulin.deng@ipst.gatech.edu; Tel: +1 404 894 5759; Postal address: 500 10th Street, NW, Atlanta, Georgia, 30318, United States)

Abstract

A uniquely-structured dye-sensitized solar cell was fabricated by assembling two photoanodes and one counter electrode in a single compartment. The two photoanodes have complementary roles in absorbing solar light at different wavelengths. The power conversion efficiency of the hybrid cell can reach to 6.6%, which is significantly higher than that of the single cell. The rational design of the hybrid cell does not need interconnecting layer as that is used in conventional tandem solar cells, leading to higher power conversion efficiency.

Dye-sensitized solar cells (DSSCs) have been studied extensively because of their low cost compared to Si based solar cells¹. Great effort has been made to improve their power conversion

efficiency to sharpen their competitive edge over Si based solar cells²⁻¹². Different methods have been adopted to realize better power conversion efficiency. One attempt is to develop a high-efficiency dye which can absorb as much light as possible in intensity and over a broader solar spectrum^{13,14}. However, it is difficult to achieve high photoelectric conversion and low charge recombination at the same time for high-efficiency dye design. Another method is to use simultaneous or stepwise co-sensitization of multiple dyes for cell fabrication¹⁵⁻¹⁸. Co-sensitization compensates the disadvantages of absorption limitation of a single dye and broadens solar wavelength absorption range. However, in the simultaneously co-sensitized DSSCs^{19,20}, there is an absorption competition between different dyes, and possible negative interaction between these dyes also occurs. As a result, the total light conversion is only slightly improved or even lowered than a single dye-sensitized DSSC. While in the case of stepwise co-sensitization on DSSCs²¹⁻²⁵, two or more different dye-sensitized semiconductor layers (usually TiO₂ or ZnO) will be coated stepwise on a conductive substrate. Clearly, with the increase of the semiconductor thickness, difficulties will be encountered for successful injection of electrons to the conductive substrate.

Tandem or hybrid solar cells are also used to harvest more solar energy^{26,27}. Generally, these cells were fabricated by vertically stacking two or more subcells connected by an interconnecting layer. Tandem/hybrid cells have the advantages of broadening the absorption spectrum and avoiding negative interaction among dyes. Nelles et al. designed tandem DSSCs with red dye and black dye in the upper and lower compartments, respectively²⁸. However, in their design, the incident light needs to pass through multiple electrodes, including two working electrodes and one semitransparent counter electrode, to reach the lower dye. This would reduce the light absorption of the bottom cell. Murayama and Mori designed a face to face tandem cell

structure with two dye-sensitized TiO_2 at each side as working electrodes and a platinum mesh in the middle as the counter electrodes²⁹. Homogeneous DSSC (N3 dye-sensitized TiO_2) and heterogeneous DSSC (N3 dye and black dye-sensitized TiO_2) were tested in this design, with power conversion efficiency being 1.8% and 3.9%, respectively. Likewise, the middle counter electrode, or called interconnecting layer, would block the part of solar energy, leading to the low efficiency. Yamaguchi et al. fabricated tandem dye-sensitized solar cells on a glass rod, in which two different dye-sensitized TiO_2 layers were assembled along the glass rod.³⁰ These tandem cells showed a low power conversion of 1.33%. The reason for the low efficiency was because that almost of the light passed through the glass rods directly without being absorbed. Only a small portion of the light contacting the interface between the glass rod and the TiO_2 /dye layer was used for photoconversion.

Although tandem solar cells commonly have higher efficiency than a single solar cell, there are many challenges in order to further improve their performance. For example, to connect two or more subcells in a series, interconnecting layers have to be used. Ideally, the interconnecting layers should have sufficient conductivity, high transparency, good uniformity and high chemical stability. Their energy levels should also match with those of donor/acceptor molecules in the active layer. Unfortunately, such ideal interconnecting layers have not been reported. Besides, compared to solid polymer tandem solar cells, the liquid electrolyte based dye sensitized tandem solar cells are more difficult to be fabricated due to the leakage of the electrolyte.

Herein, we report a uniquely-structured dye-sensitized solar cell that has double-layered photoanodes with two different dyes, but only one counter cathode as shown in Figure 1. Different from traditional DSSCs, a second photoanode layer is inserted between traditional anode (with N719 sensitized TiO_2 nanoparticles) and platinum cathode in our novel design. This

second photoanode layer is made by a porous and electrical conducting Ti/Ni mesh with a thin layer of dye-sensitized TiO₂ nanoparticles coated on it. The two photoanodes containing different dyes are assembled face-to-face and connected in a parallel mode as co-anodes. Since the second layer is supported by a porous Ti/Ni mesh, the electrolyte can easily diffuse through this layer to reach the cathode. Because of the two different dye-sensitized TiO₂ layers, such rationally designed hybrid solar cells can absorb more light over a broader wavelength.

Our double-layered DSSCs are different from conventional tandem solar cells. In our design, there is only one cathode but two parallel connected photoanodes coated with different dyes. The hybrid cells designed in this study allows the incident light to directly reach the second photoanode after passing through the first one, which can reduce the loss of solar energy and internal resistance. More importantly, no interconnecting electrode is needed, which overcomes the bottleneck in fabricating tandem cells. Furthermore, the single-compartment design renders the cells to be more compact and of lower internal resistance. For our hybrid DSSCs, two photoanodes could be separately prepared, thereby eliminating the issues encountered by co-sensitized solar cells.

Figure 1 illustrates a schematic diagram of the structure of hybrid solar cells. The top photoanode is made of N719-sensitized TiO₂ on ITO glass. The second photoanode is composed of N749-sensitized TiO₂ on the substrate of porous Ti/Ni mesh (i.e., 500nm Ti was sputtered on Ni mesh). The whole cell compartment is filled with electrolyte solution. The two dyes, N719 and N749, compensate the light absorption range so the solar cell efficiency can be substantially improved. The electrons in the highest occupied molecular orbital (HOMO) of N719 and N749 are excited and injected to TiO₂ nanoparticles and then transport to the ITO and Ti/Ni mesh, respectively. The redox couple in the electrolyte will receive the electrons at the counter

electrode and reduce the dye molecules back to their original states. The photo of the hybrid cell is shown in Figure 1(b).

The SEM images of Ti/Ni mesh is shown in Figure 2(a). Clearly, the Ti/Ni mesh is made up of interconnected holes with diameters in the range of 100-250 μm . The porous nature of Ti/Ni mesh is an essential prerequisite for the electrolyte to penetrate through the whole space in the solar cell compartment. Figure 2(b) displays the morphology of TiO₂ nanoparticles(NP) thin film coated on Ti/Ni mesh. The TiO₂ NP thin film appears to have some cracks, which are beneficial for electrolyte to flow through. Figure 2(c) shows the SEM image of the TiO₂ NP. It can be seen that the diameters of TiO₂ NP are ranged from 20 to 40nm. Nano-sized pores can be seen among TiO₂ nanoparticles. These nano-sized pores can provide passways for the diffusion of electrolyte and the adsorption of dye molecules.

Figure 3 shows the X-ray diffraction profile of the TiO₂ nanoparticles. Both anatase and rutile phase exists in the as-prepared TiO₂ nanoparticles. The strong diffraction peaks at 25° and 48°, corresponding to face (101) and (200), respectively, are solid evidence of TiO₂ NP in its anatase phase. The strong peaks at 27°, 36°, 55°, corresponding to face (110), (101), (211), respectively, indicate the existence of rutile phase of TiO₂ NP. All peaks are in good agreements with the standard spectrum of anatase and rutile TiO₂. (JCPDS no. 84-1286 and 88-1175).

To impart the hybrid cell with higher power conversion efficiency than an individual cell, the sensitizers on the two photoanodes should have complementary absorption spectrum for solar energy. Thus, the UV-Vis absorption spectra and IPCE spectra of N719 and N749 sensitized solar cells were measured, as shown in Figure 4(a) and (b). UV-Vis spectra in Figure 4(a) showed that N719 sensitized solar cells have a strong absorption band in the range of 500-800nm with maximum peak $\lambda=556\text{nm}$ was observed; N749 sensitized solar cells have two peaks in the

range of 400-500nm and 600-800nm, with maximum peaks at $\lambda=450\text{nm}$ and $\lambda=647\text{nm}$ were detected. In Figure 4(b), the IPCE spectra of individual N719 and N749 show peaks in the similar positions as compared to UV-Vis spectra. Compared with the N749 IPCE spectra with N719 spectra, a stronger absorption was observed in the range of 600-800nm. The IPCE of the hybrid cell indicates better absorption across the broad spectral range. These results suggest that the N719 sensitized TiO_2 absorbs solar energy in the shorter wavelength region firstly, and then the longer wavelength light is further captured by the N749 sensitized TiO_2 in the second photoanode. The two dyes used in this study nearly cover the whole panchromatic spectra in the range of visible light.

The photocurrent density–voltage (J–V) characteristics of the individual N719 sensitized solar cell on ITO glass (N719 cell), individual N749 sensitized solar cell on Ti/Ni mesh (N749 cell) and the hybrid cell are compared in Figure 5(a). The important parameters, including open-circuit voltage V_{oc} , short-circuit current density J_{sc} , fill factor FF, and power conversion efficiency η are summarized in Table 1. The short-circuit current density (J_{sc}) at one sun illumination (standard illumination at AM1.5, or 1 kW/m^2) for the hybrid cell is $13.8\text{ mA}\cdot\text{cm}^{-2}$, which is much higher than either of the single cell, i.e. $9.2\text{ mA}\cdot\text{cm}^{-2}$ for N719 cells and $8.84\text{ mA}\cdot\text{cm}^{-2}$ for N749 cells. The significant increase in J_{sc} reflects the parallel-connected nature of the hybrid cell and also substantiates the results of UV-VIS spectrum, suggesting that the hybrid cell can capture a nearly panchromatic spectrum of the sun light. It is interesting to see that the V_{oc} of the hybrid cell is close to the average of single cells V_{oc} . (i.e. $V_{oc\text{-hybrid}} \approx 1/2(V_{oc\text{-cell1}} + V_{oc\text{-cell2}})$). Lee et al.³¹, Miao et al.³² and Nelles et al.²⁸ carried out similar experiments on multi-layered TiO_2 with different dyes but by other methods. The relationship between V_{oc} of the

whole cell and that of each single in their research agrees with the results in our experiments.

The V_{oc} of a DSSC can be calculated by the following equation,

$$V_{oc} = \frac{RT}{\beta F} \ln\left(\frac{AI}{n_0 k_b [I_3^-] + n_0 k_r [D^+]}\right),$$

where R is the molar gas constant, T is the temperature, F is the Faraday constant, β is the reaction order for I_3^- and electrons, A is the electrode area, I is the incident photon flux, n_0 is the concentration of accessible electronic states in the conduction band, and k_b , k_r are the kinetic constants of the backreaction of the injected electrons with triiodide and the recombination of these electrons with oxidized dyes (D^+), respectively. Since the loss term as $n_0 k_r [D^+]$ can be neglected and $[I_3^-]$ can be considered as constant, V_{oc} depends logarithmically on $1/k_b$, ($k_b = \omega_{max}^{33}$, where ω_{max} refers to the peak frequency of the second arc). From the results of electrochemical impedance spectroscopy (EIS) shown in Figure 5(b), the peak frequency of for the hybrid cell (ω_{max}) is 7.15Hz, which is in the middle of those of single cells. (i.e., $\omega_{max} = 18.62\text{Hz}$ for N719 cell and $\omega_{max} = 4.98\text{Hz}$ for N749 cell). This explains why the V_{oc} for hybrid cells are in between of those of N719 cells and N749 cells. Besides using Ti/Ni mesh as the substrate for the second photoanode, stainless steel mesh (SSM) was also tested. However, the V_{oc} of SSM cell can only reach a value of 4.9V, with power conversion efficiency of 0.96%. The possible reason for the unsatisfactory performance of SSM cell is that the SSM can be oxidized into Fe oxides at high temperature (around 500°C) during sintering³⁴⁻³⁶, which greatly accelerates the back recombination of electrons at the TiO_2 /dye/electrolyte interface. Thus, we adopted Ti/Ni mesh as the substrate for the bottom cell in our hybrid cell.

Notably a fill factor of 0.56 was measured for the hybrid cell, which is lower than that of N719 cell and N749 cell. The lower FF of hybrid cell is probably due to the higher internal

resistance compared to the single cell. The overall energy conversion efficiency for hybrid cell is 6.6%, which is 21% (compared to N719 cell) and 47% (compared to N749 cell) higher than the single cell. The significant improvement in the efficiency of hybrid cell proves that within the same dye-sensitized TiO₂ areas, the performance of the hybrid cell is much better than a single cell.

To study the kinetics of electron transport and recombination, electrochemical impedance spectroscopy (EIS) and an equivalent circuit were studied in Figure 5b. The key parameters obtained from EIS measurements are listed in Table 2. Each EIS curve consists of two arcs. The first arc assigned at high frequency scan region is related to the kinetics at the interface of Pt counter electrode/electrolyte. The diameter of the first arc is regarded as the resistance at the Pt surface (R_{ct1}), which is 20 Ω (N719 cell), 22 Ω (N749 cell), and 24 Ω (hybrid cell), respectively in our experiments. The similar R_{ct1} for the three cells agrees with the fact that the Pt counter electrodes are prepared under the same condition. The second arc in the curve is assigned at low frequency region, indicating the kinetics at the interface of TiO₂/dye/electrolyte. The diameter of the second arc is related to charge-transfer resistance for electron recombination (R_{ct2}), which is 56 Ω (N719 cell), 120 Ω (N749 cell), and 62 Ω (hybrid cell), respectively. Obviously, the charge combination resistance of the hybrid cell is in between the two individual cells. This is not surprising as the hybrid cells combine the characteristics of individual N719 cell and N749 cells. Consequently the properties will be compromised. For the same principle, the effective recombination rate constant(k_b) and effective electron lifetime(τ_b) of the hybrid cells also locate in between of the single cells. R_s represent the serious resistance of the circuit. It is reasonable to see that the series resistance of the hybrid cell is higher than either of the single cell.

Conclusions

In conclusion, uniquely-structured dye-sensitized solar cells have been rationally designed and implemented by assembling two photoanodes (i.e., ITO/TiO₂ and Ti/Ni mesh/TiO₂) and one Pt/ITO counter electrode in a single compartment. The power conversion efficiency of the hybrid cell (6.6%) is significantly higher than that of single cell. The higher J_{sc} of the hybrid cell substantiates the signature of the parallel cell connection. The porous structure of the second photoanode enables the crafting of hybrid cell in a single compartment, by allowing the electrolyte to diffuse through the whole cell space. In sharp contrast to other hybrid/tandem cells which need the interconnecting layers, the two photoanodes were designed to be right next to each other, thereby eliminating the unnecessary loss of solar energy. As such, our study demonstrates an easy and scalable method to craft hybrid dye-sensitized solar cells with improved power conversion efficiency.

Acknowledgements

Xiaodan Zhang would like to thank the Institute of Paper Science and Technology at Georgia Tech to provide financial support.

Notes and References

1. B. Oregan and M. Gratzel, *Nature*, 1991, **353**, 737-740.
2. U. Bach, D. Lupo, P. Comte, J. E. Moser, F. Weissortel, J. Salbeck, H. Spreitzer and M. Gratzel, *Nature*, 1998, **395**, 583-585.
3. E. J. W. Crossland, N. Noel, V. Sivaram, T. Leijtens, J. A. Alexander-Webber and H. J. Snaith, *Nature*, 2013, **495**, 215-219.
4. A. Yella, H. W. Lee, H. N. Tsao, C. Y. Yi, A. K. Chandiran, M. K. Nazeeruddin, E. W. G. Diau, C. Y. Yeh, S. M. Zakeeruddin and M. Gratzel, *Science*, 2011, **334**, 629-634.

5. M. D. Ye, D. J. Zheng, M. Q. Lv, C. Chen, C. J. Lin and Z. Q. Lin, *Advanced Materials*, 2013, **25**, 3039-3044.
6. M. D. Ye, H. Y. Liu, C. J. Lin and Z. Q. Lin, *Small*, 2013, **9**, 312-321.
7. Y. H. Jang, X. K. Xin, M. Byun, Y. J. Jang, Z. Q. Lin and D. H. Kim, *Nano Letters*, 2012, **12**, 1742-1742.
8. J. Wang and Z. Q. Lin, *Chemistry-an Asian Journal*, 2012, **7**, 2754-2762.
9. X. K. Xin, J. Wang, W. Han, M. D. Ye and Z. Q. Lin, *Nanoscale*, 2012, **4**, 964-969.
10. J. Wang and Z. Q. Lin, *Chemistry of Materials*, 2010, **22**, 579-584.
11. M. D. Ye, X. K. Xin, C. J. Lin and Z. Q. Lin, *Nano Letters*, 2011, **11**, 3214-3220.
12. X. K. Xin, M. He, W. Han, J. H. Jung and Z. Q. Lin, *Angewandte Chemie-International Edition*, 2011, **50**, 11739-11742.
13. C. H. Siu, C. L. Ho, J. He, T. Chen, X. N. Cui, J. Z. Zhao and W. Y. Wong, *Journal of Organometallic Chemistry*, 2013, **748**, 75-83.
14. N. Humphry-Baker, K. Driscoll, A. Rao, T. Torres, H. J. Snaith and R. H. Friend, *Nano Letters*, 2012, **12**, 634-639.
15. J. Chang, C. P. Lee, D. Kumar, P. W. Chen, L. Y. Lin, K. R. J. Thomas and K. C. Ho, *Journal of Power Sources*, 2013, **240**, 779-785.
16. C. L. Lee, W. H. Lee and C. H. Yang, *Journal of Materials Science*, 2013, **48**, 3448-3453.
17. G. D. Sharma, M. K. Panda, M. S. Roy, J. A. Mikroyannidis, E. Gad and A. G. Coutsolelos, *Journal of Renewable and Sustainable Energy*, 2013, **5**.
18. N. C. Jeong, H. J. Son, C. Prasittichai, C. Y. Lee, R. A. Jensen, O. K. Farha and J. T. Hupp, *Journal of the American Chemical Society*, 2012, **134**, 19820-19827.
19. C. Magne, M. Urien and T. Pauporte, *Rsc Advances*, 2013, **3**, 6315-6318.

20. V. Saxena, P. Veerender, A. K. Chauhan, P. Jha, D. K. Aswal and S. K. Gupta, *Applied Physics Letters*, 2012, **100**.
21. G. D. Sharma, S. P. Singh, R. Kurchania and R. J. Ball, *Rsc Advances*, 2013, **3**, 6036-6043.
22. H. Choi, S. Kim, S. O. Kang, J. J. Ko, M. S. Kang, J. N. Clifford, A. Forneli, E. Palomares, M. K. Nazeeruddin and M. Gratzel, *Angewandte Chemie-International Edition*, 2008, **47**, 8259-8263.
23. C. M. Lan, H. P. Wu, T. Y. Pan, C. W. Chang, W. S. Chao, C. T. Chen, C. L. Wang, C. Y. Lin and E. W. G. Diau, *Energy & Environmental Science*, 2012, **5**, 6460-6464.
24. K. M. Lee, Y. C. Hsu, M. Ikegami, T. Miyasaka, K. R. J. Thomas, J. T. Lin and K. C. Ho, *Journal of Power Sources*, 2011, **196**, 2416-2421.
25. F. Inakazu, Y. Noma, Y. Ogomi and S. Hayase, *Applied Physics Letters*, 2008, **93**.
26. Z. M. Beiley and M. D. McGehee, *Energy & Environmental Science*, 2012, **5**, 9173-9179.
27. W. S. Jeong, J. W. Lee, S. Jung, J. H. Yun and N. G. Park, *Solar Energy Materials and Solar Cells*, 2011, **95**, 3419-3423.
28. M. Durr, A. Bamedi, A. Yasuda and G. Nelles, *Applied Physics Letters*, 2004, **84**, 3397-3399.
29. M. Murayama and T. Mori, *Journal of Physics D-Applied Physics*, 2007, **40**, 1664-1668.
30. J. Usagawa, S. S. Pandey, S. Hayase, M. Kono and Y. Yamaguchi, *Applied Physics Express*, 2009, **2**.
31. K. Lee, S. W. Park, M. J. Ko, K. Kim and N. G. Park, *Nature Materials*, 2009, **8**, 665-671.
32. Q. Q. Miao, L. Q. Wu, J. N. Cui, M. D. Huang and T. L. Ma, *Advanced Materials*, 2011, **23**, 2764-2768.
33. M. Adachi, M. Sakamoto, J. T. Jiu, Y. Ogata and S. Isoda, *Journal of Physical Chemistry B*, 2006, **110**, 13872-13880.
34. M. G. Kang, N. G. Park, K. S. Ryu, S. H. Chang and K. J. Kim, *Chemistry Letters*, 2005, **34**, 804-805.
35. L. J. Meng, M. X. Wu, Y. M. Wang, W. Guo, C. Y. Ma, T. L. Ma and R. Silva, *Applied Surface Science*, 2013, **275**, 222-226.

36. F. Y. Ouyang and W. L. Tai, *Applied Surface Science*, 2013, **276**, 563-570.

Figures:

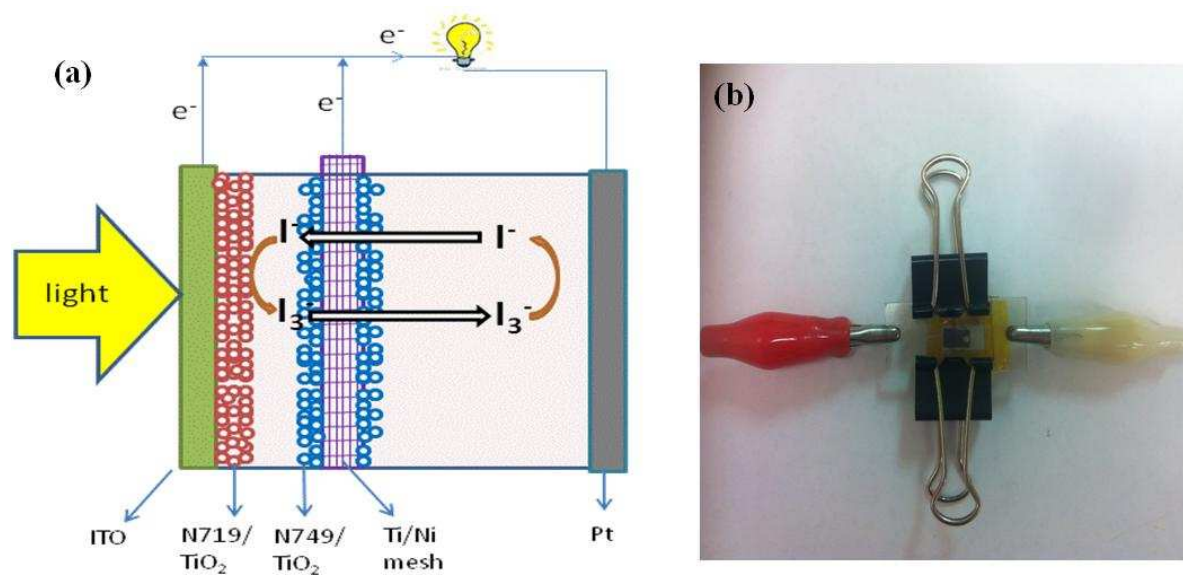


Figure 1. (a) Schematic illustration of dye-sensitized solar cells with double-layered photoanodes. (b) Photo of the hybrid cell device.

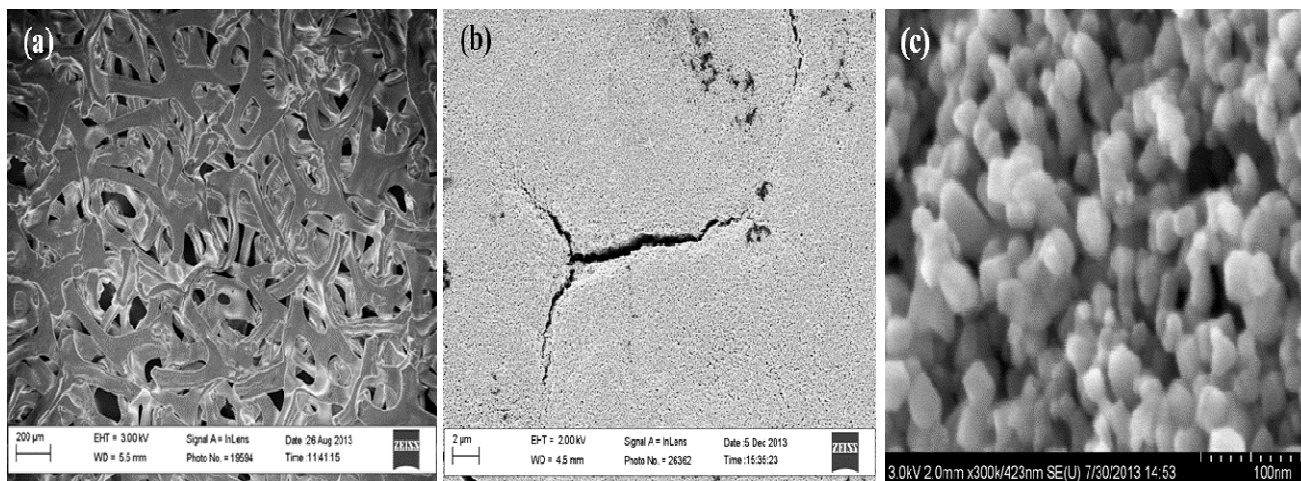


Figure 2. SEM images of (a) Ti/Ni mesh; (b) TiO₂ nanoparticles on Ti/Ni mesh; (c) TiO₂ nanoparticles on ITO glasses.

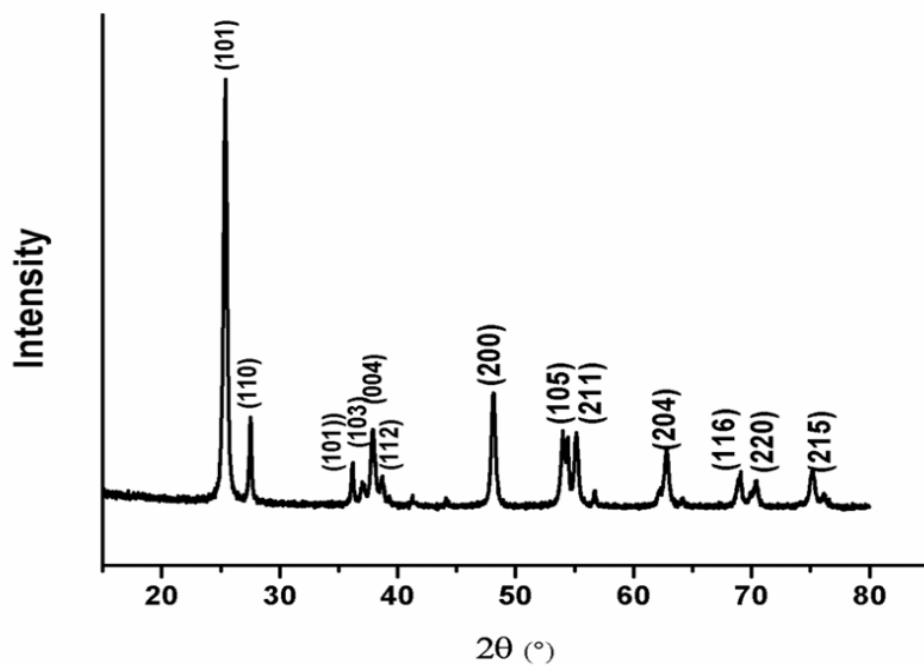


Figure 3. X-ray diffraction patterns of TiO₂ nanoparticles.

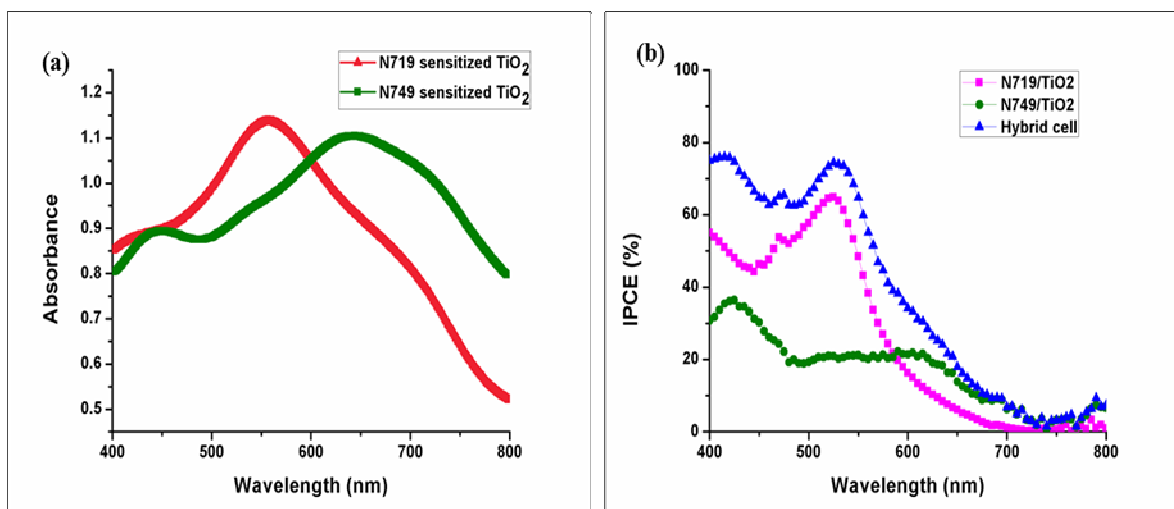


Figure 4. (a) UV-Vis spectrum of N719/TiO₂ film and N749/TiO₂ film. (b) IPCE spectra of N719-sensitized TiO₂ cell, N749-sensitized TiO₂ cell, and the hybrid cell.

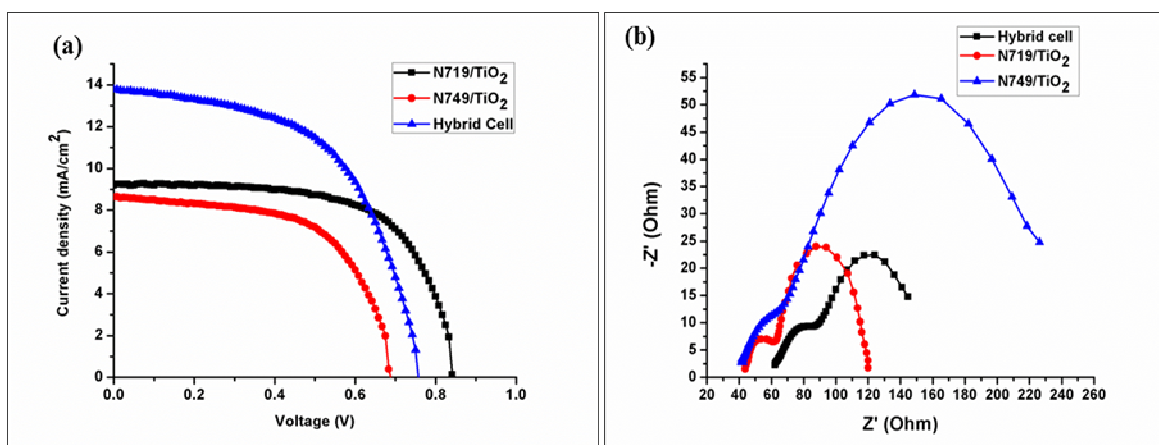


Figure 5. (a) Photocurrent density-voltage (J-V) curves of individual N719-sensitized TiO₂ cell (black line), individual N749-sensitized TiO₂ cell (red line), and the hybrid cell (blue line). (b) Electrochemical impedance spectroscopy of individual N719-sensitized TiO₂ cell (red line), individual N749-sensitized TiO₂ cell (blue line), and the hybrid cell (black line). The equivalent circuit is inserted in the bottom right of the figure.

Table 1. Photovoltaic parameters of the hybrid cell and the individual N719 and N749 cells.

| | V_{oc} (V) | J_{sc} ($\text{mA}\cdot\text{cm}^{-2}$) | FF | η (%) |
|-------------|--------------|---|------|------------|
| N719 cell | 0.84 | 9.2 | 0.66 | 5.2 |
| N749 cell | 0.69 | 8.64 | 0.61 | 3.5 |
| Hybrid cell | 0.76 | 13.8 | 0.56 | 6.6 |

Table 2. Parameters determined by the electrochemical impedance spectroscopy measurement.

| | k_b (s^{-1}) | τ_b (s) | R_s (Ω) | R_{ct1} (Ω) | R_{ct2} (Ω) |
|-------------|---------------------------|--------------|--------------------|------------------------|------------------------|
| N719 cell | 18.62 | 0.054 | 41 | 20 | 56 |
| N749 cell | 4.98 | 0.200 | 52 | 24 | 120 |
| Hybrid cell | 7.15 | 0.140 | 62 | 22 | 62 |

k_b : effective rate constant for recombination reaction.

τ_b : effective electron lifetime for recombination.

R_s : series resistance

R_{ct1} : charge transfer resistance related to the recombination of electrons.

R_{ct2} : resistance at the Pt surface.